Application of image flow cytometry for the characterization of red blood cell morphology

Ruben N. Pinto[ab], Joseph A. Sebastian[ac], Michael Parsons[d], Tim C. Chang[e], Jason P. Acker[fg] and Michael C. Kolios[ab]

[a]Institute of Biomedical Engineering, Science and Technology (iBEST), Toronto, Canada
[b]Department of Physics, Ryerson University, Toronto, Canada
[c]Department of Electrical & Computer Engineering, Ryerson University, Toronto, Canada
[d]Lunenfeld-Tanenbaum Research Institute (LTRI), Sinai Health System, Toronto, Canada
[e]MilliporeSigma, a business of Merck KGaA, Seattle, WA
[f]Centre for Innovation, Canadian Blood Services, Edmonton, Canada
[g]Department of Laboratory Medicine and Pathology, University of Alberta, Edmonton, Canada

ABSTRACT

Red blood cells (RBCs) stored in hypothermic environments for the purpose of transfusion have been documented to undergo structural and functional changes over time. One sign of the so-called RBC storage lesion is irreversible damage to the cell membrane. Consequently, RBCs undergo a morphological transformation from regular, deformable biconcave discocytes to rigid spheroechinocytes. The spherically shaped RBCs lack the deformability to efficiently enter microvasculature, thereby reducing the capacity of RBCs to oxygenate tissue. Blood banks currently rely on microscope techniques that include fixing, staining and cell counting in order to morphologically characterize RBC samples; these methods are labor intensive and highly subjective. This study presents a novel, high-throughput RBC morphology characterization technique using image flow cytometry (IFC). An image segmentation template was developed to process 100,000 images acquired from the IFC system and output the relative spheroechinocyte percentage. The technique was applied on samples extracted from two blood bags to monitor the morphological changes of the RBCs during *in vitro* hypothermic storage. The study found that, for a given sample of RBCs, the IFC method was twice as fast in data acquisition, and analyzed 250-350 times more RBCs than the conventional method. Over the lifespan of the blood bags, the mean spheroechinocyte population increased by 37%. Future work will focus on expanding the template to segregate RBC images into more subpopulations for the validation of the IFC method against conventional techniques; the expanded template will aid in establishing quantitative links between spheroechinocyte increase and other RBC storage lesion characteristics.

Keywords: Blood bag, discocyte, image flow cytometry, image segmentation, morphology characterization, red blood cell, RBC morphology, red cell concentrate, spheroechinocyte, storage lesion

1. INTRODUCTION

With over 85 million red blood cell (RBC) units consumed annually, RBC transfusion is the most frequent procedure carried out within transfusion medicine[1]. The primary goal of RBC transfusion is to augment the oxygen carrying capability of a compromised cardiovascular system. Using specialized separation techniques, blood banks extract RBCs from donated whole blood and suspend them in a preservative solution[2]. This red cell concentrate (RCC) is stored in a sterile blood bag at hypothermic temperatures until used for transfusion. The *in vitro* shelf life has been set at a maximum of 42 days for RBCs suspended in a saline-adenine-glucose-mannitol (SAGM) preservative under storage temperatures of 1-6°C[3]. The storage duration was based on standard guidelines specifying that 1) a maximum of 1% *in vitro* percentage hemolysis (RBC rupturing) and 2) a minimum of 75% percent *in vivo* survivability (24 hours post transfusion) must be observed on the last storage day[4].

High-Speed Biomedical Imaging and Spectroscopy: Toward Big Data Instrumentation and Management II
edited by Kevin K. Tsia, Keisuke Goda, Proc. of SPIE Vol. 10076, 100761F · © 2017 SPIE
CCC code: 1605-7422/17/$18 · doi: 10.1117/12.2253583

While these criteria provide some information on the quality of RBCs that remain in circulation after transfusion, they lack the ability to assess the functional capacity of the transfused RBCs. It has been well documented that during *in vitro* storage, biochemical and biomechanical changes in RBCs (collectively termed as RBC storage lesions) lead to deleterious effects in cell function and viability[5-7]. One of the consequences of the RBC storage lesion is the loss of cell membrane integrity, which leads to irreversible damage and impaired *in vivo* functionality[8]. Due to a hypothermic storage environment, the glycolysis pathways slow down and cause a shortage of ATP for basic cellular function[9]. Lacking a constantly replenished supply of ATP *in vitro*, reductases lose the capacity to effectively combat the accumulation of oxidative products. The lengthened presence of anionic radicals leads to the damage of phospholipids and proteins that are responsible for membrane structure[10]. To counteract this increasing oxidative stress, RBCs begin the removal of damaged cell membrane via vesiculation[11,12]. Under *in vitro* storage conditions, however, these products remain within the same supernatant that suspends the RBCs. RBCs under this continuous biochemical stress gradually morph from regular biconcave discocytes into smaller, more rigid spherical objects with membranous projections[8]. Morphologically termed as spheroechinocytes, these RBCs lack the deformability to efficiently enter capillary networks, reducing their capacity to deliver oxygen to the microvasculature[13].

Hemolysis and cell survivability studies are unable to evaluate the morphological state of intact RBCs. In blood banks, a morphological assay based on light-microscopy determines the impact of the RBC storage lesion on cell shape[14]. Samples of RCC are diluted, smeared, fixed and stained on slides to be viewed under a light microscope; 100 cells are randomly chosen for morphological characterization by observation[15]. Spheroechinocytes are visually detected by markers that include a spherical shape, spiky surface projections, relatively small diameter and lack of central pallor[16,17]. The morphology assay measures the number of spheroechinocytes (as a percentage), providing an indication of the effect of the RBC storage lesion on the morphology. This measure of the *in vitro* quality of the RBC sample can infer its capacity to transport oxygen *in vivo*.

The light-microscopy morphology assay provides an insight into the functional capacity of a sample of RCC. However, it is a laborious process that is prone to subjective bias. Flow cytometry possesses the potential to overcome some of these limitations. The technology rapidly assesses large cell populations for multiple parameters, using signals from the transmitted and scattered light from each cell[18]. It has been shown that the intensities of forward and side scatter can be correlated with cell size and internal heterogeneity, respectively[19]. Furthermore, fluorescent tagging can be used to acquire further details on contents of the cell membrane or cytosol. Flow cytometry is superior to light microscopy in the speed and automation available for measurement and statistical analysis, however, lacks in an ability to provide images for differentiating morphological changes.

Image flow cytometry (IFC) combines the complementary techniques of light microscopy and conventional flow cytometry. IFC incorporates a bright field light source, microscope objectives and high-quality CCD cameras into a conventional flow cytometry platform to respectively produce the illumination, magnification and spatial sensitivity necessary for image capture[20]. Paired with an integrated image analysis package, IFC expands on the analytical capabilities available in conventional flow cytometry, while providing automation and speed that is impractical for conventional light microscopy. Specifically, IFC provides the image resolution and morphological content of light microscopy, along with large sample size, automation and population statistics provided by flow cytometry[21].

This paper presents a novel RBC morphology assay using the Amnis ImageStream®X Mark II IFC system (MilliporeSigma), and a customized image segmentation template developed within the Amnis IDEAS® software package (version 6.2.64). The morphology assay and template are shown to process 100,000 images to select only focused, single cell, front view RBC images (~25,000 – 35,000), from which the relative spheroechinocyte population percentage is calculated. This automated, high throughput technique is applied to samples of two RCC blood bags over their lifespan to monitor the morphological RBC changes as a function of storage time.

2. METHODS

2.1 RCC blood bags

Two RCC blood bags were transported from Canadian Blood Services (CBS) blood-for-research center (netCAD, Vancouver, Canada) to the Institute of Biomedical Engineering, Science and Technology (iBEST, Toronto, Canada).

Throughout the 15-20 hour transit period, the bags were insulated in standard blood shipment containers which are comprised of a styrofoam /cardboard box filled with ice packs to maintain hypothermic temperatures. The RCC provided in blood bags were separated from anticoagulated whole blood using a top/bottom manufacturing method, leukoreduced and stored in up to 110 ml of SAGM preservative solution. Upon reception, blood bags were promptly stored in a designated laboratory fridge until six weeks after the production date. Before the first sample extraction for IFC analysis, bags were fitted with a sampling site coupler that contained a natural rubber sleeve stopper for needle penetration.

2.2 IFC morphology assay

In a biosafety cabinet, 1.5 ml aliquots of RCC were extracted with 20-gauge needles via the coupler. This method was repeated to collect three individual samples (per bag) into *safe*PICO syringes, which contained a vented cap to expel air within the sample and seal the sample from the external environment (Radiometer, Copenhagen, Denmark). The syringes were placed in a plastic pouch, covered in bubble wrap and placed in a cooled styrofoam box for transportation to the ImageStream$^{®X}$ IFC system. Syringe samples were placed in an adjacent refrigerator until required for measurement.

From each syringe, an RCC aliquot of 5µl was diluted with 200µl of phosphate-buffered saline in a vial, which was placed into the ImageStream$^{®X}$ sample holder for automated aspiration and image acquisition. 100,000 images were captured, per sample, at a low speed and high sensitivity fluidics mode and under 60× image magnification. Post acquisition, the syringes and excess RCC samples were discarded as per biosafety guidelines. The experiments were performed at approximately 10 day intervals until the expiration date of the blood bags.

2.3 Data analysis

All raw data files were transferred via USB to a portable hard drive to be uploaded onto a computer with a Windows 7 64 bit OS, consisting of an Intel Core i7-4790 processor and a 16 GB memory. Each raw data file was opened on the IDEAS® software platform and was processed automatically by the developed RBC image segmentation template (Section 3.1). The processed file displayed the relative percent fraction of spheroechinocytes within the analyzed population.

3. RESULTS/DISCUSSION

3.1 RBC image segmentation template

Figure 1 outlines the gating strategy used to exclude unwanted subpopulations (represented by images A, B, C, F and G) from the analysis. The goal was to create an image segmentation template based on a series of mask/feature combinations to automatically differentiate front view discocyte (images D, E) from front view spheroechinocyte subpopulations (images H, I). In general, feature values for individual images were calculated from the intensity distribution of pixels enclosed by an underlying object mask. The segregation of RBC images into subpopulations was carried out in five steps (Figures 2-6). Since each dot on a plot was addressable to an image, subpopulation gates based on regions of interest (ROIs) could be visually verified. Furthermore, tagged RBCs that were representative of certain RBC subtypes were chosen in consultation with an RBC morphology expert (T. Turner, CBS, Edmonton, Canada). Once overlaid onto plots containing the entire population, these *truth populations* were used as a guide to refine subsequent gates and ROIs.

Figure 2 shows a histogram used to discriminate between unfocused and focused images, as illustrated in section I (Figure 1). The feature *gradient RMS* calculates the root mean square (RMS) of the intensity gradient between pixels within the image mask[22]. Compared to focused images, unfocused and blurred images lacked sharp changes in intensity, thereby producing lower *gradient RMS* values. By visual verification, images with *gradient RMS* values below 54 were excluded from further analysis.

Figure 3 displays the plot used to discriminate between single and multi-cell images, as illustrated in section II (Figure 1). Here the *aspect ratio* feature, calculated as the ratio of the object's minor axis over its major axis, was plotted against the *area* feature based on the size of the object in square microns[22]. Both features used the default bright field object mask. A gate was created such that object aggregates within the same image field were excluded from further analysis.

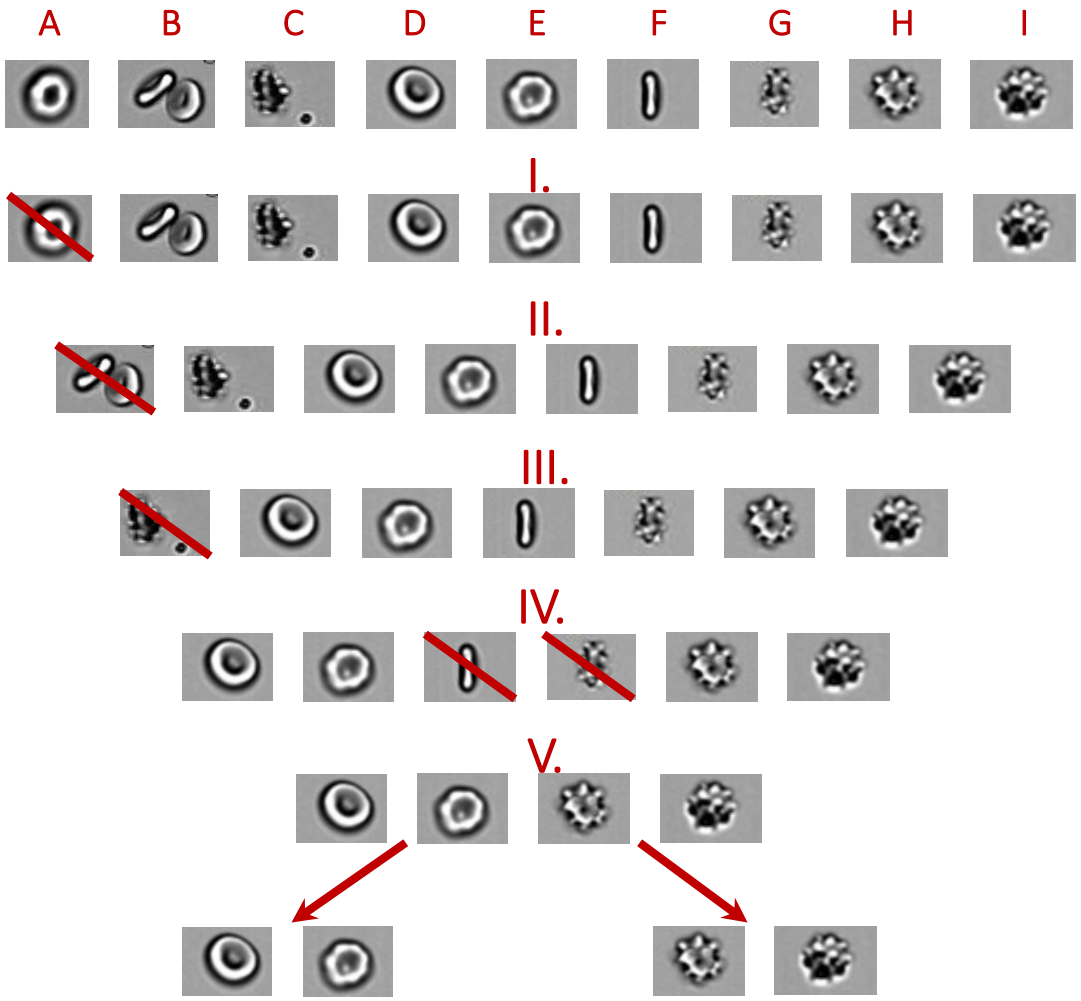

Figure 1: *(Top Row)* Typical RBC images produced by the ImageStream$^{®X}$ IFC system, including unfocused (A), multi-cell (B), cells with calibration beads (C), front view discocytes (D, E), side view discocytes (F), side view spheroechinocytes (G) and front view spheroechinocytes (H, I). *(Second Row and Below)* Sequential gating based on various mask/feature combinations was used to exclude objects of type A (I.), B (II.), C (III.), F and G (IV.), and differentiate populations D and E from H and I to classify discocytes and spheroechinocytes, respectively.

While multi-cell images were excluded from further analysis (Figure 3), a small but significant fraction of object images containing calibration beads (speed beads) were not successfully removed (image C, section II, Figure 1). The presence of these beads impaired mask application and subsequent feature analysis and therefore needed to be removed.

Figure 4 displays the plot used to discriminate between images containing RBCs with calibration beads and single RBC images, as illustrated in section III (Figure 1). Here the *area* feature was plotted against the *circularity* feature to show the relative size of the object in relation to its deviation from a circle[22]. A gate was created to exclude images containing RBCs with calibration beads from subsequent analysis.

Figure 5 displays the plot used to discriminate between front view and side view RBC images, as illustrated in section IV (Figure 1). The IDEAS® *feature finder* tool was used to statistically determine the best features to discriminate front view and side view RBC images. To do this, approximately 50-100 truth populations were chosen for both front and side view RBC images. The *feature finder* calculated the RD mean (*Fisher's discriminant ratio*) – the difference in the means divided by the sum of the standard deviations for the two populations - for each feature[22]. Features with higher RD values equated

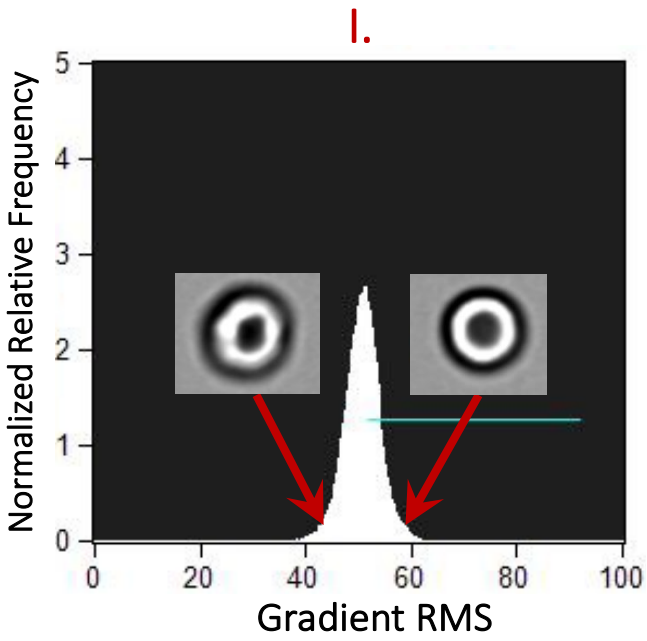

Figure 2: (see section I, Figure 1); histogram of gradient RMS (counts of normalized relative frequency) within the default bright field mask. Inset images provide examples of unfocused (left) and focused (right) RBC images. Value of gradient RMS of images are indicated by red arrows. Images containing gradient RMS values above 54 were selected for further analysis (horizontal light blue line).

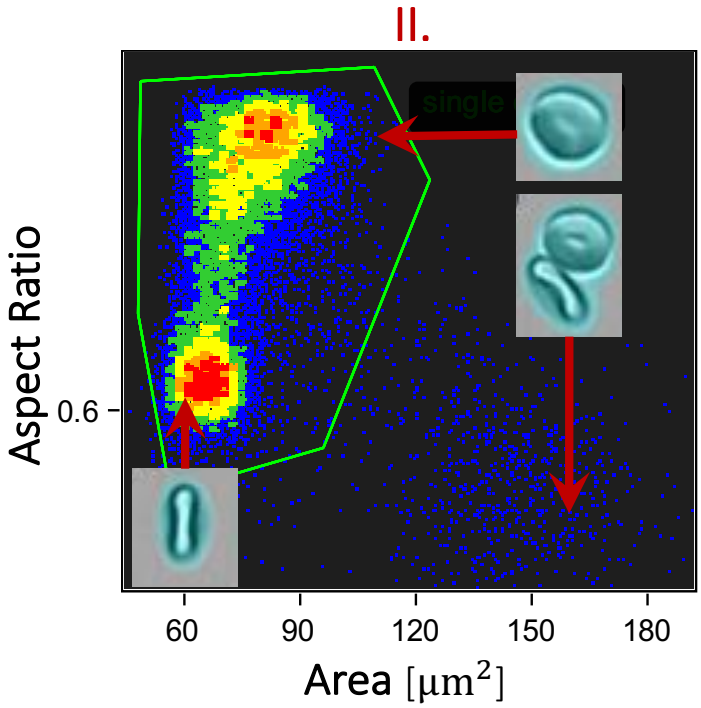

Figure 3: (see section II, Figure 1); plot of aspect ratio versus area using the default bright field mask. Inset images provide examples of front view (top right), multi-cell (middle right) and side view (bottom left) RBC images. Object masks are highlighted in light blue. Red arrows point to the location of images within the scatter plot. Color scale consists of, in order of increasing relative population density: blue, green, yellow, orange, red. A gate based on images within the ROI (light green boundary) was selected for further analysis.

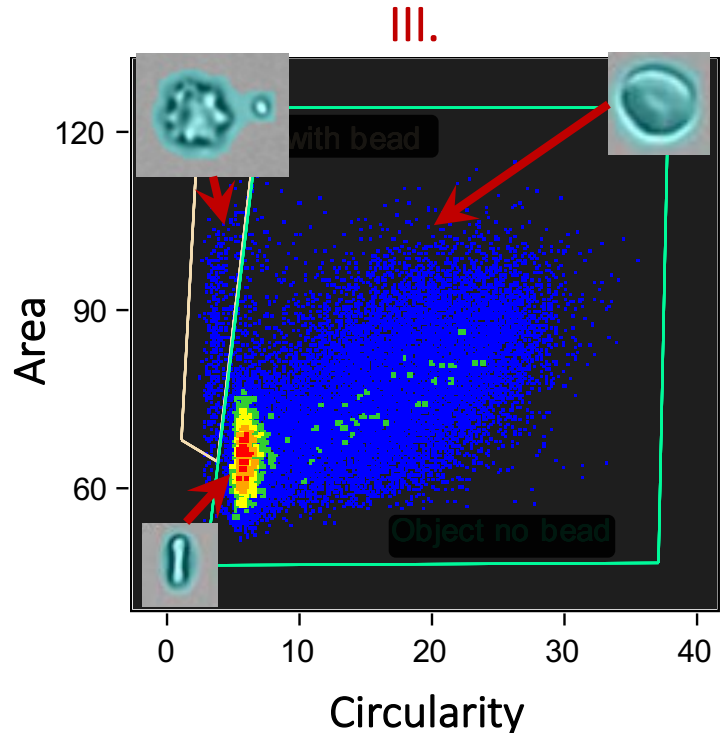

Figure 4: (see section III, Figure 1); plot of area versus circularity using the default bright field mask. Inset images provide examples of cells with calibration beads (top left), front view (bottom right) and side view (bottom left) RBC images. Object masks are highlighted in light blue. Red arrows point to the location of images within the scatter plot. The color scale consists of, in order of increasing relative population density: blue, green, yellow, orange, red. A gate based on images within the right-side ROI was selected for further analysis.

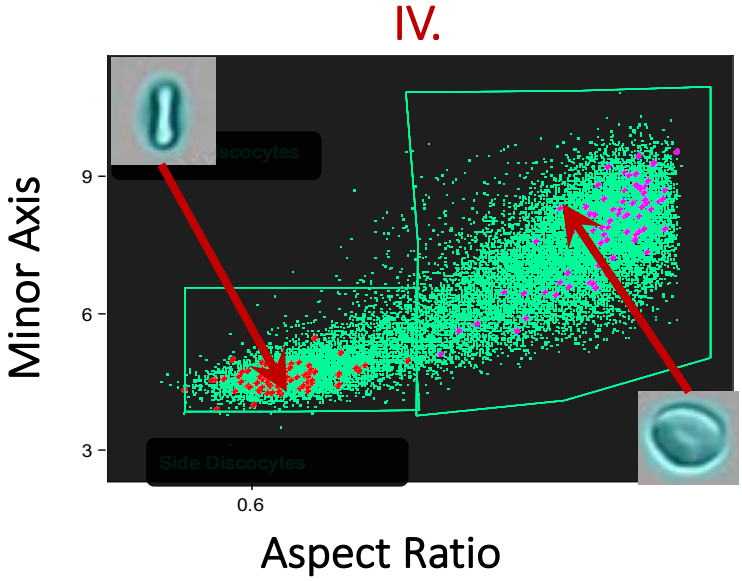

Figure 5: (see section IV, Figure 1); plot of minor axis vs. aspect ratio using the default bright field mask. Inset images provide examples of the front view (bottom right) and side view (top left) RBC images. Object masks are highlighted in light blue. Red arrows point to the location of images within the scatter plot. Sample images (light green) are overlaid with truth populations of the front view (purple) and side view (red) images. A gate based on images within the right-side ROI was selected for further analysis.

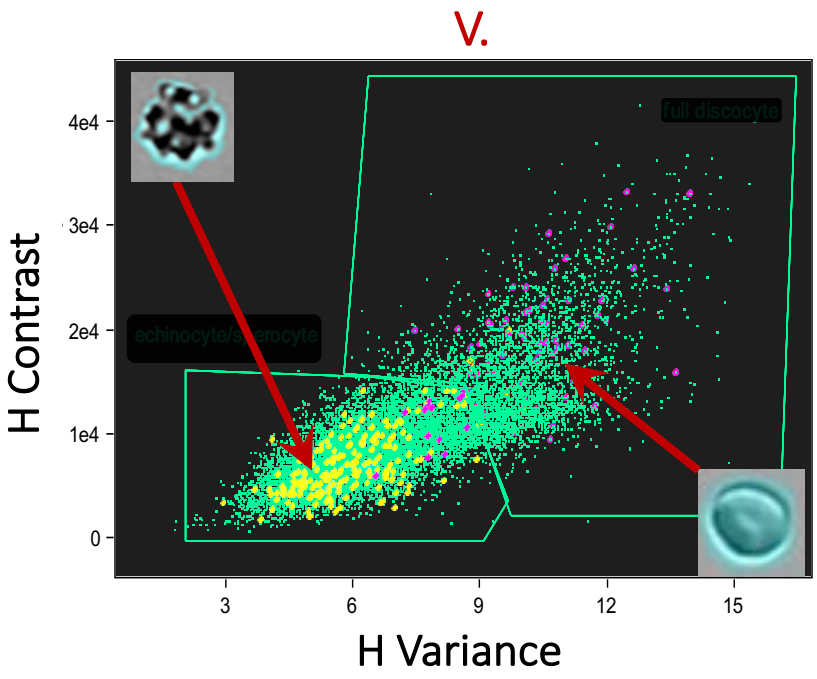

Figure 6: (see section V, Figure 1); plot of H contrast versus H variance using the default bright field mask. Inset images provide examples of front view discocyte (bottom right) and front view spheroechinocyte (top left) RBC images. Default bright field masks are highlighted in light blue. Red arrows point to the location of images within the scatter plot. Sample images (light green) are overlaid with truth populations of the front view discocytes (purple) and front view spheroechinocytes (yellow) images. A gate based on truth populations segregated the two subpopulations.

to higher discriminatory power and hence better subpopulation separation. In this way, it was determined that *aspect ratio* and *minor axis* features would provide good discrimination between front and side view RBCs.

The IDEAS® default bright field masks enclosing side view images (Figure 1: C, D) could not provide sufficient detail to segregate discocytes and spheroechinocytes using the *feature finder*. Side view images were hence excluded from analysis. On average, approximately 40% of the single cell image population consisted of side view images. The general trends in discocyte/spheroechinocyte population changes over time are speculated to be unaffected by the exclusion of this subpopulation; however, this exclusion poses limitations when interpreting any quantitative analysis of discocyte/spheroechinocyte populations. Future work will investigate masks that contour the cell boundary more tightly without losing necessary image detail.

Figure 6 displays the plot used to discriminate between front view discocyte and spheroechinocyte images, as illustrated in section V (Figure 1). A similar strategy employing the *feature finder* tool (Figure 5) was used to determine the best features to discriminate front view discocytes and front view spheroechinocytes. The strongest statistical discriminators were found to be *Haralick (H) contrast* and *H variance*[22]. These parameters were named after a set of texture features defined by Haralick et al. to normalize and characterize the local variation in intensity distribution within the masks[23]. A key contributor to normalized local variance in RBC images was the central pallor present in discocyte images. Hence, the resulting *H contrast* versus *H variance* plot placed the central pallor-lacking masks of spheroechinocyte images towards the lower left corner.

3.2 Image acquisition and processing speed

Upon loading one RCC vial for automated aspiration into the ImageStream$^{®X}$, a raw image data file was generated in approximately 5 minutes. Each saved raw data file contained 100,000 brightfield images and took up approximately 500MB of storage space. Uploading and automated processing of the raw data file using the morphology template (Section 3.1) took under 5 minutes. Assuming that the measuring apparatus and hardware are within one location, the relative fraction of spheroechinocytes within a sample population of approximately 25,000-35,000 cells could be acquired in less than 15 minutes after RCC extraction. In contrast, the light-microscopy morphology assay requires roughly half an hour after RCC extraction to acquire the relative fraction of spheroechinocytes within a sample of 100 cells. Evidence for the potential advantages of this automated RBC morphology characterization technique is provided through the enhancement in acquisition and processing speed.

3.3 Time-series study

Figure 7 plots the IFC time series measurements of the spheroechinocyte population percentages acquired from two RCC blood bags (labeled 1 and 2, dashed lines). Also plotted on the figure are average RBC populations used for analysis, which ranged between 25,000 and 35,000 images (solid line). During the lifespan of bags 1 and 2, template processing of IFC images measured an average spheroechinocyte population increase of 38.7% and 35.5% respectively. Both bags were measured to have a starting spheroechinocyte percentage of 55.7% on day 2; however, the percentage values may differ if the side view RBC images are included in the analysis (Section 3.1). One hypothesis to explain the variation in the rate of spheroechinocyte population growth between the bags was that the rate might potentially be dependent on the quality of RBCs provided by the donor. It is suggested that by tracking the rate of change of spheroechinocyte population, the severity of the RBC storage lesion may be assessed. To test this hypothesis, future work will concentrate on establishing quantitative links between spheroechinocyte population increase and other characteristics of the RBC storage lesion.

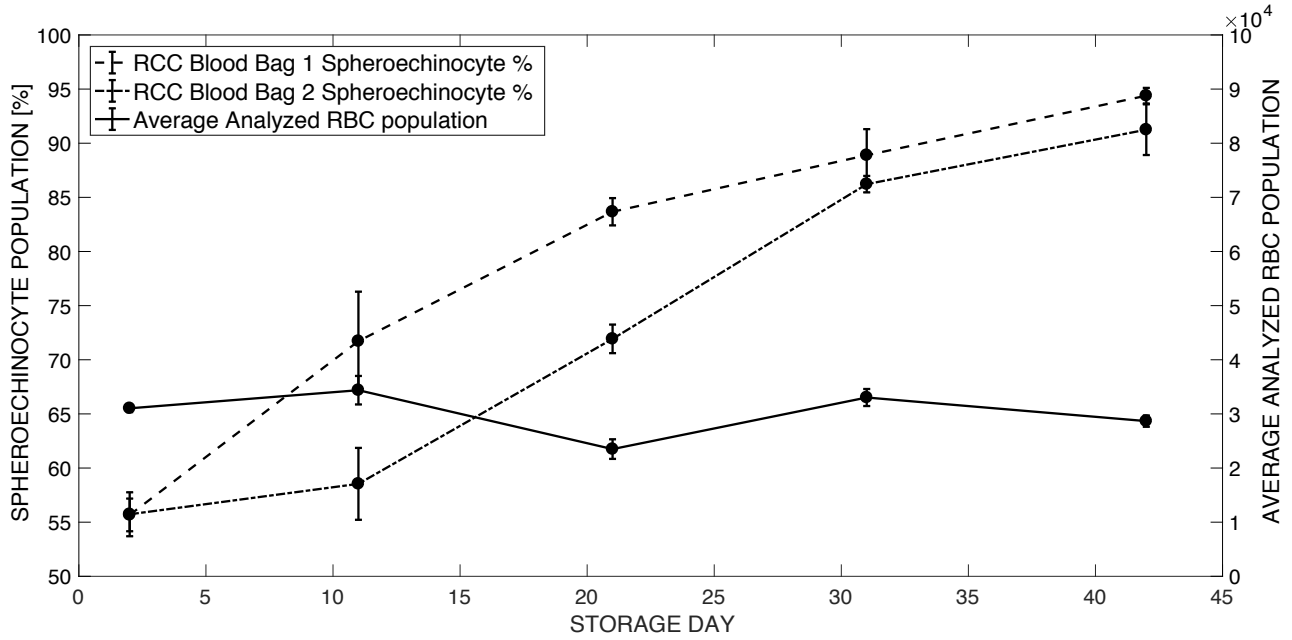

Figure 7: Average analyzed RBC populations (solid) and spheroechinocyte population percentages of samples of RCC blood bags 1 (dashed) and 2 (dash-dotted) as a function of storage day. Error bars represent the standard deviation of 3 samples.

Validation against current lab techniques is necessary. Conventional morphology assessments segregate RBCs into six subcategories and use a morphology index to provide a measure of sample quality[2,14]. Future work will expand on the current template to segregate RBCs into these six subcategories, which will involve improving masks to contour cell

membranes more closely (Section 3.1). Using this improved image segmentation template, the IFC method can be compared to the conventional techniques to determine the level of agreement. Furthermore, the inclusion of side view images for analysis (Section 3.1) can allow for a quantitative investigation of the influence of donor characteristics on RBC quality.

4. CONCLUSIONS

This paper presents the potential of using IFC as a highly automated, statistically robust and objective technique for morphologically characterizing RBCs, in contrast to current methods that are labor intensive and are highly subjective. An image segmentation template was developed on the IDEAS® software platform to determine the relative spheroechinocyte population percentage. Measurements showed a spheroechinocyte population increase of 38.7% and 35.5% for two RCC blood bags over the 42-day preservation period. Variation in the rate of change of spheroechinocyte population suggests that this parameter may potentially be donor-dependent; however, such inferences are limited by the fact that side view images of RBCs could not be included in the analysis. Compared to the conventional method, this novel technique was found to have a significantly faster image acquisition and processing speed. More significantly, the 250-350 times increase in the analyzed sample size allows for an improvement in the statistical robustness of morphological characterization.

Future work will concentrate on improving the masks used to select RBCs for analysis. The current template will be expanded to segregate RBCs into six subpopulations; this new template will be used to validate the IFC method against conventional techniques. Quantitative links between results obtained from the IFC method and current techniques in the characterization of RBC storage lesions will be investigated. It is thought that the monitoring of RBC morphology distribution change as a function of time can provide an indication of the RBC storage lesion severity in RCC blood bags during storage.

ACKNOWLEDGMENTS

Funding for this project was provided through a Collaborative Health Research Projects (CHRP) grant (application # 315271), a joint initiative between the Natural Sciences and Engineering Research Council of Canada (NSERC) and the Canadian Institutes of Health Research (CIHR) awarded to the principle investigators M. C. Kolios and J. P. Acker. T.R. Turner is gratefully acknowledged for consultations associated with the development of the RBC image segmentation template. The Lunenfeld Tanenbaum Research Institute (LTRI) flow cytometry facility is acknowledged for providing access for image flow cytometry experiments.

REFERENCES

[1] Carson, J. L., et al., "Red blood cell transfusion: a clinical practice guideline from the AABB," Ann. Intern. Med. 157(1), 49-58 (2012).
[2] Acker, J. P., et al., "A quality monitoring program for red blood cell components: in vitro quality indicators before and after implementation of semiautomated processing," Transfusion 54(10), 2534-2543 (2014).
[3] Högman, C. F., et al., "Red cell Suspensions in SAGM Medium. Further experience of in vivo survival of red cells, clinical usefulness and plasma-saving effects," Vox Sang. 45(3), 217-223 (1983).
[4] Dumont, L. J., and AuBuchon, J. P., "Evaluation of proposed FDA criteria for the evaluation of radiolabeled red cell recovery trials," Transfusion 48(6), 1053-1060 (2008).
[5] Gabrio, B. W., et al., "Erythrocyte preservation. I. The relation of the storage lesion to in vivo erythrocyte senescence," J. Clin. Invest. 33(2), 242-246 (1954).
[6] Högman, C. F. and Meryman, H. T., "Storage parameters affecting red blood cell survival and function after transfusion," Transfus. Med. Rev. 13(4), 275-296 (1999).
[7] D'Alessandro, A., et al., "Red blood cell storage: the story so far," Blood Transfus. 8(2), 82-88 (2010).
[8] Bessis, M., Weed, R.I. and Leblond, P. F., [Red cell shape: Physiology, Pathology, Ultrastructure], Springer Verlag, New York, Heidelberg and Berlin, 35-37 (1973).
[9] Hess, J. R., "Red cell changes during storage," Transfus. Apher. Sci. 43(1), 51-59 (2010).
[10] Chaudhary, R. and Katharia, R., "Oxidative injury as contributory factor for red cells storage lesion during twenty-eight days of storage," Blood Transfus. 10(1), 59-62 (2012).
[11] Antonelou, M. H., et al., "Effects of pre-storage leukoreduction on stored red blood cells signaling: a time-course evaluation from shape to proteome," Journal Proteomics 76, 220-238 (2012).

[12] Salzer, U., et al., "Vesicles generated during storage of red cells are rich in the lipid raft marker stomatin," Transfusion 48(3), 451-62 (2008).
[13] Frank, S.M., "Decreased erythrocyte deformability after transfusion and the effects of erythrocyte storage duration," Anesth. Analg. 116(5), 975–981 (2013).
[14] Usry, R. T., Moore, G. L., and Manalo, F. W., "Morphology of stored, rejuvenated human erythrocytes," Vox Sang. 28(3), 176-183 (1975).
[15] Tchir, J. D. R., Acker, J. P. and Holovati, J. L., "Rejuvenation of ATP during storage does not reverse effects of the hypothermic storage lesion," Transfusion 53(12), 3184-3191 (2013).
[16] Palmer, L., et al., "ICSH recommendations for the standardization of nomenclature and grading of peripheral blood cell morphological features," Int. J. Hematol. 37(3), 287-303 (2015).
[17] Longster, G. H., et al., "Scanning electron microscope studies of red cell morphology," Vox Sang. 22(2), 161-170 (1972).
[18] Watson, J. V., "The early fluidic and optical physics of cytometry," Cytometry Part A 38(1), 2-14 (1999).
[19] Shapiro, H. M., [Practical flow cytometry, 4th Ed.], John Wiley & Sons, New Jersey, 2-12 (2003).
[20] Sklar, L. A., [Flow Cytometry for Biotechnology], Oxford University Press, New York, 57-67 (2005).
[21] McGrath, K. E., Bushnell, T. P., and Palis, J., "Multispectral imaging of hematopoietic cells: where flow meets morphology," J. Immunol. Methods. 336(2), 91-97 (2008).
[22] Amnis Corporation, [Image data exploration and analysis software user's manual, Version 4.0], Seattle, 123-205 (2009).
[23] Haralick, R.M., Shanmugan, K. and Dinstein, I., "Textural Features for Image Classification," IEEE Trans. Syst., Man, Cybern., Syst. 3(6), 610-621 (1973).